Propagation direction of geodesic acoustic modes driven by drift wave turbulence

Propagation direction of geodesic acoustic modes driven by drift wave turbulence

M. Sasaki[1, 2], K. Itoh[2, 3, 4], T. Kobayashi[4], N. Kasuya[1, 2], A. Fujisawa[1, 2], and S.-I. Itoh[1, 2, 5]

[1]Research Institute for Applied Mechanics, Kyushu University, Kasuga 816-8580, Japan
[2]Research Center for Plasma Turbulence, Kyushu University, Kasuga 816-8580, Japan
[3]Institute of Science and Technology Research, Chubu University, Kasugai 487-8501, Japan
[4]National Institute for Fusion Science, Toki 509-5292, Japan
[5]Department of Innovative Energy Science and Engineering, Graduate School of Engineering, Chubu University, Kasugai, Japan

Abstract

Selection rule of the radial propagation direction of geodesic acoustic modes (GAMs) is investigated. Here, we study the influence of nonlinear coupling with drift wave turbulence on propagation direction of GAMs. Based on wave-kinetic equation for the turbulence, the phase-space dynamics is numerically solved and the nonlinear saturated states are obtained, where the phase-space consists of the real space and the wavenumber space. A wave pattern of the GAM in a nonlinear saturated state varies to form a standing wave, outward and inward propagating waves, depending on the peak radial wavenumber of the turbulence. The impact of nonlinear coupling with turbulence is discussed by deriving the GAM dispersion relation that includes the effect of the turbulence.

Keywords: zonal flows, GAMs, propagation, dispersion relation, turbulence trapping, drift wave

1 Introduction

Investigation of characteristics of macro-scale flows generated by micro-scale turbulence is one of important subjects in the studies of magnetically confined plasmas. There are several kinds of the flow driven by the turbulence such as the poloidal mean flow, toroidal rotation, and the zonal flows [1, 2]. In toroidal plasmas, zonal flow has oscillatory branch, geodesic acoustic mods (GAMs) [3]. The GAMs play important roles for improving the plasma confinement, such as turbulence suppression [4], ion heating [5], and the toroidal rotation drive [6]. Recently, a new role of the GAM for the turbulence propagation

has been proposed: the GAM traps clumps of turbulence and the trapped turbulence propagates radially with the phase velocity of the GAM [7]. A possibility has been discussed that the trapped turbulence, carried by the GAM, deteriorates the transport barrier [8]. Thus, the effect of the GAMs on bulk plasmas differs, depending on the propagation direction. Therefore, it is necessary to understand theoretically how the radial propagation direction of the GAM is determined.

Radial propagation of the GAMs has been observed experimentally in several devices [9]-[21]. Unidirectional outward propagating GAMs have been observed in JFT-2M [9], TEXTOR [11], DIII-D [13], HL-2A [14], JET [15], and COMPASS [16]. Inward propagation of the GAMs has been observed in FT-2 [17], and ASDEX-Upgrade [18]. Standing wave or coexistence of the inward and outward propagation has been observed in HT-7 [19], ISTTOK [20], TUMAN-3M [21], and ASDEX Upgrade [18]. The standing wave patterns has been observed near the separatrix due to the boundary effect has been observed in JFT-2M [9, 10, 12]. In turbulence simulations, the coexistence of the inward and outward propagating GAMs [4, 22], and outgoing propagation [23] have been observed. The linear dispersion relation of the GAMs, which includes the plasma geometrical effect [24, 25], and the temperature gradient effect [26, 27, 28], has been investigated. The turbulence effects on the frequency shift has been studied [29, 30]. However, a sign asymmetry of the radial wavenumber for the nonlinear drive by the turbulence has not been studied, which is important for the selection rule for the radial propagation direction of the GAMs.

In this study, we investigate the selection rule for the propagation direction of the GAMs, focusing on the impact of the turbulence. The wave-kinetic equation for the turbulence and the fluid equation for the GAM are numerically solved, keeping the phase-space dynamics of the turbulence (turbulence trapping effect), where the phase-space consists of the real space and the wavenumber space. A wave pattern of the GAM in a nonlinear saturated state varies to form a standing wave, outward and inward propagating waves, depending on the peak radial wavenumber of the turbulence. We derive the GAM dispersion relation with the effect of the turbulence in order to discuss the turbulence effect. The rest of the paper is organized as follows. The model equations are introduced in section 2. The simulation results on the nonlinear evolution of the GAM and turbulence, and the GAM propagation properties in nonlinear saturated states are shown in section 3. The nonlinear dispersion relation of the GAM that includes the turbulence effect is shown in section 4. The summary is given in section 5.

2 Model

We consider a high aspect ratio, circular cross-section toroidal plasma with a high safety factor and a weak magnetic shear. The toroidal coordinate (r, θ, ζ) is adopted, where $\nabla r, \nabla\theta$ and $\nabla\zeta$ are the radial, poloidal and toroidal directions, respectively. For the simplicity, we use the slab coordinate x instead of r only for the radial direction. The governing equation for the coupling of the drift wave turbulence with the GAM is as

follows [2, 7].

$$\partial_t N_k + \frac{\partial \omega_k}{\partial k_x}\partial_x N_k - k_\theta \partial_x \tilde{V}_\theta \frac{\partial N_k}{\partial k_x} = \gamma_L N_k - \Delta\omega N_k^2, \tag{1}$$

$$\partial_t^2 \tilde{V}_\theta + \omega_G^2 \tilde{V}_\theta = \partial_x \partial_t \int \frac{k_x k_\theta}{\left(1 + k_x^2 + k_\theta^2\right)^2} N_k d^2k + \mu_G \partial_x^2 \partial_t \tilde{V}_\theta. \tag{2}$$

Here, time and space are normalized by $\rho_s^{-1} V_d$ and ρ_s, where ρ_s is the ion sound gyroradius and V_d is the diamagnetic drift velocity, respectively. The normalized action of the turbulence is denoted by N_k, and ω_k is the frequency of the turbulence, where N_k is a function of x and the wavenumbers, k_x and k_θ, which are given as

$$N_k = \left(1 + k_x^2 + k_\theta^2\right)^2 |\phi_k|^2, \tag{3}$$

$$\omega_k = \frac{k_\theta}{1 + k_x^2 + k_\theta^2} + k_\theta \tilde{V}_\theta, \tag{4}$$

where ϕ_k is the normalized turbulent electrostatic potential. The turbulence frequency ω_k includes the doppler shift due to the GAM velocity, $\tilde{V}_\theta$. Here, the mean poloidal flow shear is neglected, in order to focus on the dynamics of the GAM. The linear growth rate and the nonlinear decorrelation rate of turbulence are denoted by γ_L and $\Delta\omega$, respectively. The GAM frequency is given as $\omega_G = \sqrt{2} L_n / R$, which corresponds to $\sqrt{2} c_s / R$ in the dimensional form, where L_n is the density scale length and R is the major radius. We treat ω_G as a constant parameter, assuming that the scale length of the temperature is much larger than the system size we consider, and neglecting the linear dispersion effect [31]-[33]. The viscosity for the GAM, μ_G, is introduced. In the derivation of the GAM evolution equation, we ignore the dynamic shearing effect for the driving the GAM [36], by assuming a weak magnetic shear [7]. It is noted that the dynamic shearing effect is observed to be weaker than the Reynolds stress drive in the JFT-2M tokamak [12]. It is noted that this model self-consistently includes the turbulence trapping effect, which is analytically investigated in [34, 35], and the self-nonlinearity to generate the higher harmonics [37]-[39].

We investigate the GAM propagation properties based on the coupling equations, Eqs. (1) and (2). In this study, we focus on the effect of the turbulence spectrum on the propagation of the GAM. The radial wavelength of the GAM is assumed to be much smaller than the temperature gradient scale length to ignore the temperature gradient effect, and the spatially homogeneous turbulence is considered. This condition can be obtained by giving γ_L and $\Delta\omega$ constant in space. Here, γ_L is given as

$$\gamma_L = \gamma_0 \exp\left[- \left(\frac{k_x - k_0}{\Delta k} \right)^2 \right]. \tag{5}$$

The poloidal wavenumber k_θ is conserved in the interaction with the GAMs, so that the k_θ is given as a parameter. The parameters are chosen to be $\gamma_0 = 0.5, \Delta\omega = 1.5, \Delta k = 1, k_\theta = 1, \omega_G = 0.1, \mu_G = 0.1$. The periodic boundary condition for the x-direction is adopted. In the following sections, we study the radial propagation direction of the GAMs by changing the peak wavenumber of the turbulence, k_0.

The assumptions in this study can be summarized as follows,

- geometry: a high aspect ratio, circular cross-section plasma, a high safety factor, a weak magnetic shear,
- GAM, $\omega_G(x) = const$: homogeneous temperature, neglecting the linear dispersion (polarization) effect,
- turbulence, $\gamma_L(x) = const, \Delta\omega = const$: homogeneous turbulence.

Here, we discuss the each assumption more detail. For the non-circular plasma geometry effect, the linear GAM frequency and the damping rate are affected [31]. However, the essence of the dynamics of the GAMs and the turbulence through the turbulent force is not changed. The safety factor should be high for the GAMs to be unstable, because the Landau damping of the GAMs approximately scales as e^{-q^2} [40]. The magnetic shear determines the magnitude of the dynamic shearing [36], where the strength of the dynamic shearing is proportional to the magnetic shear. In this study, we focus on the Reynolds force as the dominant driving force, by considering the week magnetic shear. For the linear GAM frequency, we adopt the simplest form (constant in space and no dispersion), in order to focus on the turbulence effect on the GAM propagation. As is discussed in section 4, the self-consistent treatment of the linear dispersion effect and the turbulence is necessary when the temperature is inhomogeneous. The spatially homogeneous turbulence is assumed for simplicity, which corresponds to the case that the scale length of the density gradient is constant within the several period of the GAM wavelength. Under these circumstances, the phase-space dynamics of the turbulence coupling with the GAMs are numerically calculated.

3 Nonlinear simulation of GAMs and turbulence

The coupling equations, Eqs. (1) and (2), are calculated numerically. The GAM propagation properties and the spatial relation between the GAM and the turbulence are described in this section.

3.1 Propagation properties of GAMs

A small perturbation is introduced to the turbulence and the GAM as the initial condition, and the time evolution of the turbulence and the GAM are investigated. A snapshot for the initial condition of the turbulence in the phase-space for the case of $k_0 = 0.8$ is shown in Fig. 1 (a), and those in the nonlinear saturated states are illustrated in Figs. 1(b)-(c) in the cases of $k_0 = 0, 0.3$ and 0.8, respectively. The initial small perturbation evolves to form the GAM structure. Here, the statistical properties of the nonlinear saturated states are independent on the initial conditions. The white line in Fig. 1 corresponds to the contour of ω_k, and the island structure due to the GAM velocity appears in the nonlinear saturated states. The turbulence trapping can be seen in the cases with $k_0 = 0$ and 0.3, where the turbulence is accumulated in the island of ω_k (which corresponds to the region with the negative curvature of the GAM velocity field) [7]. The spatio- temporal patterns of the GAM velocity and the turbulence energy at the saturated state are shown

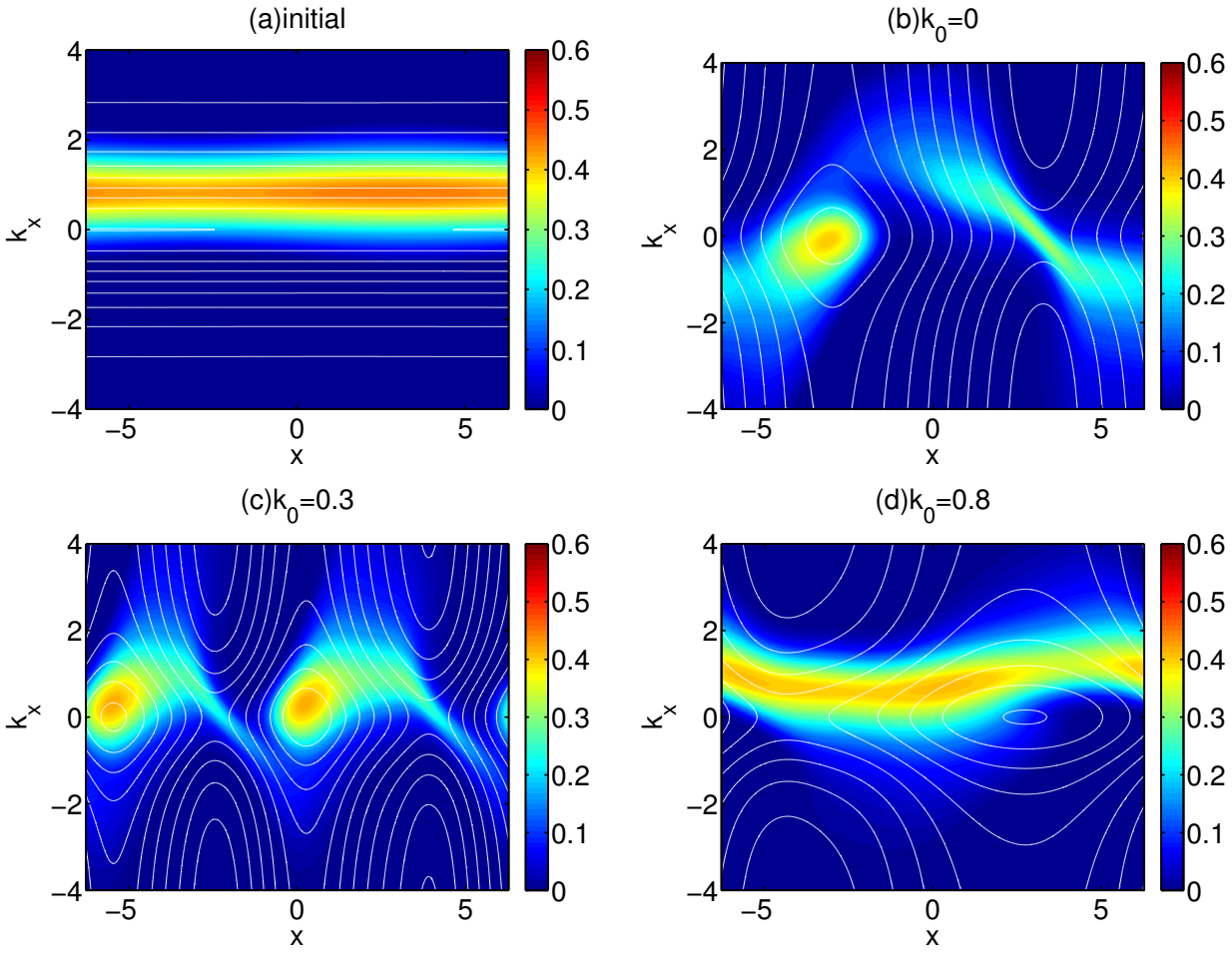

Fig. 1: Snapshots of action of turbulence, N_k, in the phase space. (a) Initial condition of N_k, and the snapshots for the nonlinear saturated states in cases of (b) $k_0 = 0$, (c) $k_0 = 0.3$, and (d) $k_0 = 0.8$ are shown, where the white line indicates the contour of ω_k. The island structure of the ω_k corresponds to the doppler shift due to the GAMs.

in Fig. 2, where the turbulence energy, I_{turb}, is calculated from $I_{turb} = \int N_k(1 + k_\perp^2)^2 dk$, where $k_\perp^2 = k_x^2 + k_\theta^2$. The standing wave pattern is obtained in the case with $k_0 = 0$, and the unidirectional propagating cases are observed in the cases of $k_0 = 0.3$ and 0.8. The wave propagates in the negative/positive radial direction in the case of $k_0 = 0.3/0.8$, respectively. In this way, the propagation direction reverses, depending on the peak turbulence wavenumber k_0.

In order to show the details of the change of the propagation direction of the GAMs, dependences of the GAM energy with the negative and positive phase velocity components on k_0 are shown in Fig. 3 (a). Here the energy of the GAM is calculated from $\mathcal{E}_{GAM} = \int \tilde{V}_\theta^2 dx$. At $k_0 = 0$, the energies of the GAM components with the positive and negative phase velocity are comparable, so that the GAM forms the standing wave. The negative phase velocity component is dominant in the region $0 < k_0 < 0.6$, and the positive phase velocity component becomes significant at $k_0 > 0.6$. The reversal of

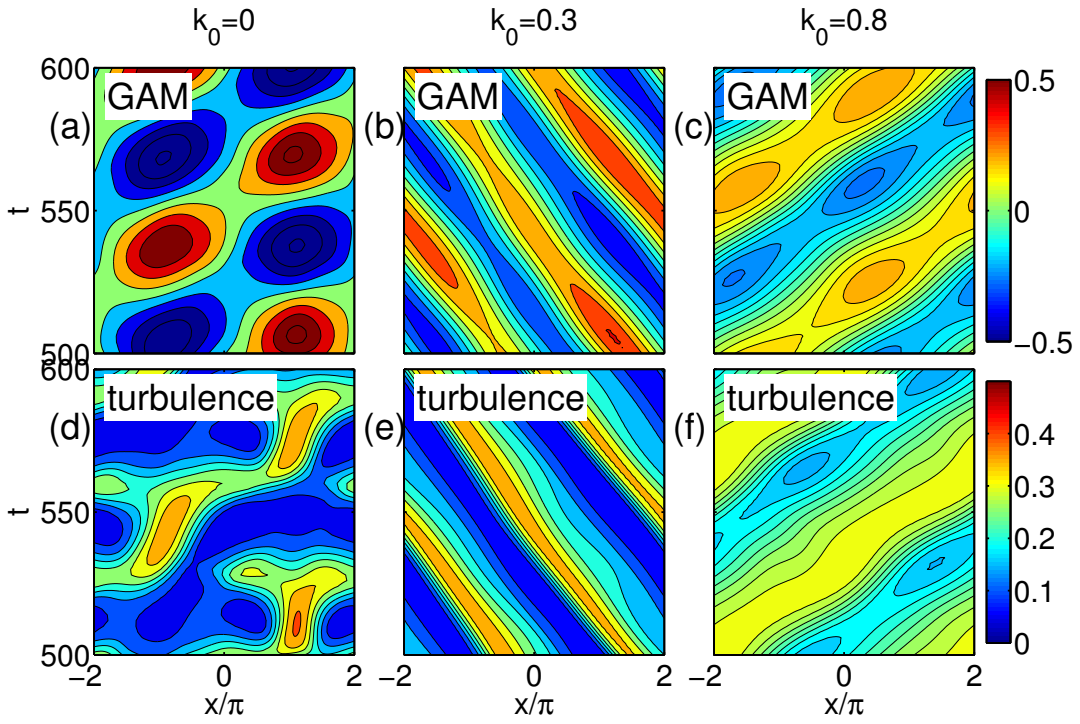

Fig. 2: Spatio-temporal behaviors of GAMs, $\tilde{V}_\theta$, and turbulence energy. The cases with $k_0 = 0, 0.3, 0.8$ are shown. Here, the turbulence energy is calculated by $I_{turb} = \int N_k(1 + k_\perp^2)^2 dk$.

the propagation direction is obtained. It should be noted that the negative propagating direction corresponds to the direction of the turbulence group velocity, which is given as $v_g = -2k_x k_\theta/(1 + k_\perp^2)^2$. We consider the spatially homogenous turbulence, so that only the turbulence propagating direction violates the symmetry for the radial direction. Of course, the propagating properties of the GAM becomes opposite when $k_0 < 0$, compared to those when $k_0 > 0$.

3.2 Spatial patterns of GAMs and turbulence: trapping effect

The spatial phase relation between the GAM and turbulence and the energy relation between them are described here. The nonlinear saturated amplitude of the GAM also changes, depending on k_0. Here, the GAMs and turbulence saturate by generating the higher harmonics through the self-nonlinearity [39, 41], which stems from the third term in the left hand side of Eq. (1). Due to the change of the amplitude of the GAM, the turbulence becomes trapped in the case with the large amplitude GAM, and the turbulence is not trapped when the amplitude of the GAM is small. Whether the turbulence is trapped or not significantly affects the spatial relation of the GAM with the turbulence,

as shown in Fig. 3 (b). The spatial phase difference, Ψ, is evaluated from

$$\Psi = \arccos\left[\frac{\int \tilde{V}_\theta \tilde{I}_{turb} dx}{\sqrt{\int \tilde{V}_\theta^2 dx}\sqrt{\int \tilde{I}_{turb}^2 dx}}\right], \tag{6}$$

where $\tilde{I}_{turb}$ is the deviation from the time average. The phase difference is small at $k_0 < 0.6$, which corresponds to the turbulence trapping states. This is because, due to the turbulence trapping, the turbulence is enhanced and suppressed in the region where $\tilde{V}_\theta > 0$ and $\tilde{V}_\theta < 0$, respectively, so that the phase difference between $\tilde{V}_\theta$ and I_{turb} becomes small. Here, the trapped turbulence in the GAM shows the bounce motion with the frequency, ω_b, which satisfies the condition, $\omega_b \gg \omega_G$, so that the trapping motion is clearly observed in these cases. The phase difference suddenly increases above $k_0 > 0.6$, which corresponds to the state without the turbulence trapping. The boundary for the trapping-untrapping region can be determined by the relation between the island width k_{island} [34] and the turbulence peak position k_0, as

$$k_{island} = \sqrt{\frac{2V_G(1+k_\theta^2)^2}{1-2V_G(1+k_\theta^2)}} > k_0 \tag{7}$$

for the turbulence trapping condition. Here, V_G is the amplitude of the GAM velocity. By using the simulation parameters, the boundary for k_0 can be estimated as $k_0 = 0.9$, which is close to the simulation result.

The energy relation between the GAM and turbulence, shown in Fig. 3 (a), can be organized by using the shearing rate of the GAM as shown Fig. 3 (c). Here the shearing rate is evaluated from the time average of $(2a)^{-1}\int_{x=-a}^{x=a}(\partial_x \tilde{V}_\theta)^2 dx$. All cases are roughly in the same trend, regardless of the cases where the turbulence is trapped in the GAM velocity field or not.

4 Dispersion relation of GAMs coupling with turbulence

In order to understand the simulation results on the GAM propagation shown in the previous section, we investigate the GAM dispersion relation with the inclusion of the turbulence effect.

We divide N_k into the mean and the linear response to the GAM as $N_k = \langle N_k \rangle + \tilde{N}_k$, where the mean turbulence is given as $\langle N_k \rangle = \gamma_L/\Delta\omega$. By replacing the time and the spatial derivatives with $-i\omega$ and iq_x, the linear response of the turbulence is obtained as

$$\tilde{N}_k = -\frac{k_\theta q_x}{\omega - q_x v_g + i\gamma_L}\frac{\partial \langle N_k \rangle}{\partial k_x} V_G. \tag{8}$$

Using this expression, the GAM dispersion relation can be written as

$$\omega^2 - \omega_G^2 + i\omega q_x^2 \mu_G - q_x^2 \omega \int \frac{k_x k_\theta^2}{(1+k_\perp^2)^2}\frac{(\omega - q_x v_g) - i\gamma_L}{(\omega - q_x v_g)^2 + \gamma_L^2}\frac{\partial}{\partial k_x}\left(\frac{\gamma_L}{\Delta\omega}\right) dk_x = 0. \tag{9}$$

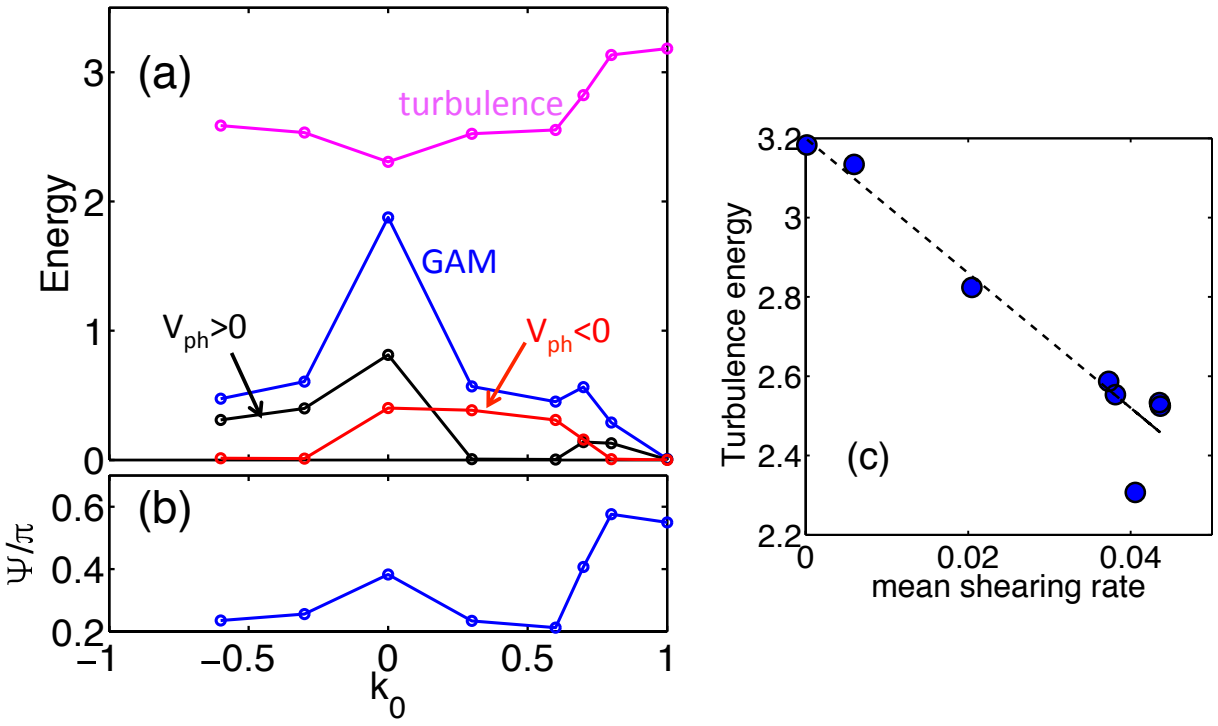

Fig. 3: (a) Dependences of energies of GAMs and turbulence on peak turbulence wavenumber, k_0. (b) Spatial phase difference between GAM and turbulence energy. (c) Relation between turbulence energy and mean shearing rate by the GAMs.

The fourth term in the left hand side of Eq. (9) is the turbulence effect, which causes the nonlinear frequency shift and the growth of the GAMs. Here, we consider the spatially homogeneous turbulence, the term with v_g is the only term to violate the symmetry for the sign of q_x. The growth rate for the positive and negative phase velocity components, $\gamma_{GAM,\pm}$, is approximately given as

$$\gamma_{GAM,\pm} \approx \frac{q_x^2 k_\theta^2 \gamma_0^2}{2\Delta\omega\Delta k^2} \int \frac{k_x(k_x-k_0)\exp\left[-2\left(\frac{k_x-k_0}{\Delta k}\right)^2\right]}{(1+k_\perp^2)^2\left\{(\omega_G \mp |q_x| v_g(k_x))^2 + \gamma_L(k_x)^2\right\}} dk_x. \tag{10}$$

By looking at Eq. (10), one can see that the driving force comes from the region $k_x < 0, k_x > k_0$, and the damping appears from $0 < k_x < k_0$. Summation of these effects determines the growth rate of the GAMs. The positive propagating component enhances the driving force from $k_x < 0$, and reduces the effect from $k_x > 0$ due to the denominator of Eq. (10), which comes from the GAM propagation effect. The negative propagating component enhances the contribution from $k_0 > 0$ (both the damping and the driving), and suppresses the effect from $k_x < 0$. Thus, the negative propagating wave becomes important, $\gamma_{GAM,-} > \gamma_{GAM,+}$, when $\Delta k/2 > k_0$, and the positive propagating wave becomes important, $\gamma_{GAM,+} > \gamma_{GAM,-}$, when $\Delta k/2 < k_0$.

The obtained dispersion relation, Eq. (9), is numerically solved. The eigenfrequency and the growth rate for the cases of $k_0 = 0.3$ and 0.8 are shown in Fig. 4. The asymmetry

in the propagation direction for the eigenfrequency and the growth rate appears. The growth rate of the negative phase velocity component is larger than that of the positive phase velocity component in the case of $k_0 = 0.3$, and only the positive phase velocity component is unstable for $k_0 = 0.8$. The frequency shift due to turbulence becomes small at the GAM radial wavenumber where the growth rate becomes maximum. This is because the growth rate becomes maximum when $\omega - q_x v_g = 0$, where this condition makes the frequency shift zero as seen in Eq. (9). Therefore, while the radial wavenumber, including its sign, is determined by the turbulence effect, the frequency shift is presumed to be dominated by the linear dispersion effect due to the higher poloidal mode couplings [31]-[33]. The growth rates for the positive and negative phase velocity components are compared in Fig. 5. The dependence of the maximum growth rate for q_x on the peak turbulence wavenumber, k_0, is shown in Fig. 5 (c). The negative propagating GAM has a larger growth rate compared to the positive propagating GAM when $k_0 < 0.6$, and the growth rate of the positive propagating GAM exceeds that of the negative propagating GAM when $k_0 > 0.6$. This tendency is consistent with the simulation results shown in the previous section. In this way, we obtain the selection rule for the propagation direction of the GAM and the turbulence clumps, which was treated as a given parameter in [34, 35], by considering the phase-space dynamics of the turbulence with the finite growth rate and nonlinear damping rate for turbulence. As is shown above, the GAM propagation direction could be closely related to the turbulence radial wavenumber spectrum. Therefore, it is important to measure the turbulence radial wavenumber spectrum simultaneous with the GAM propagations in experiments.

Finally, we discuss the global radial structure of the GAM coupling with the turbulence. From the turbulence effect, we can determine the radial direction of the phase velocity and the radial wavelength as $q_x \sim \omega_G / v_g(k_0)$, which can be obtained from the condition that the growth rate becomes maximum. Concerning to the dispersion (frequency shift dependent on the radial wavenumber), the dispersion due to the turbulence becomes small when the growth rate becomes maximum, so that the linear dispersion effect such as the ion finite orbit effect [31, 32] is dominant. Thus, when the temperature gradient effect is considered, the region where the GAM can propagate is determined from the linear dispersion; the GAM can propagate where $\omega_G(x) < \omega$ is satisfied, and the GAM is evanescent in the region of $\omega_G(x) > \omega$ [26, 27, 31]. Here, ω is the eigenfrequency. It is noted that $\omega_G(x)$ is the decreasing function of x in the case that the temperature decreases radially. Therefore, when the outward propagating wave is selected from the turbulence effect, the wave pattern is expected to be similar with the linear prediction. When the inward propagating wave is selected from turbulence effect, the GAM is presumed to be localized where the GAM obtains energy from the turbulence. In this case, the self-consistent treatment of the temperature inhomogeneity, turbulence effect and the linear dispersion effect, is required.

For the further extension of the model, we discuss the turbulence penetration into the transport barrier. The turbulence trapping by the GAM is predicted to affect the transport barrier, as in the case of the energetic particle driven GAM [8]. When the curvature of the GAM is comparable to the mean $E \times B$ flow, which is associated with the transport barrier, the GAM can screen the mean flow. Thus, the turbulence can penetrate

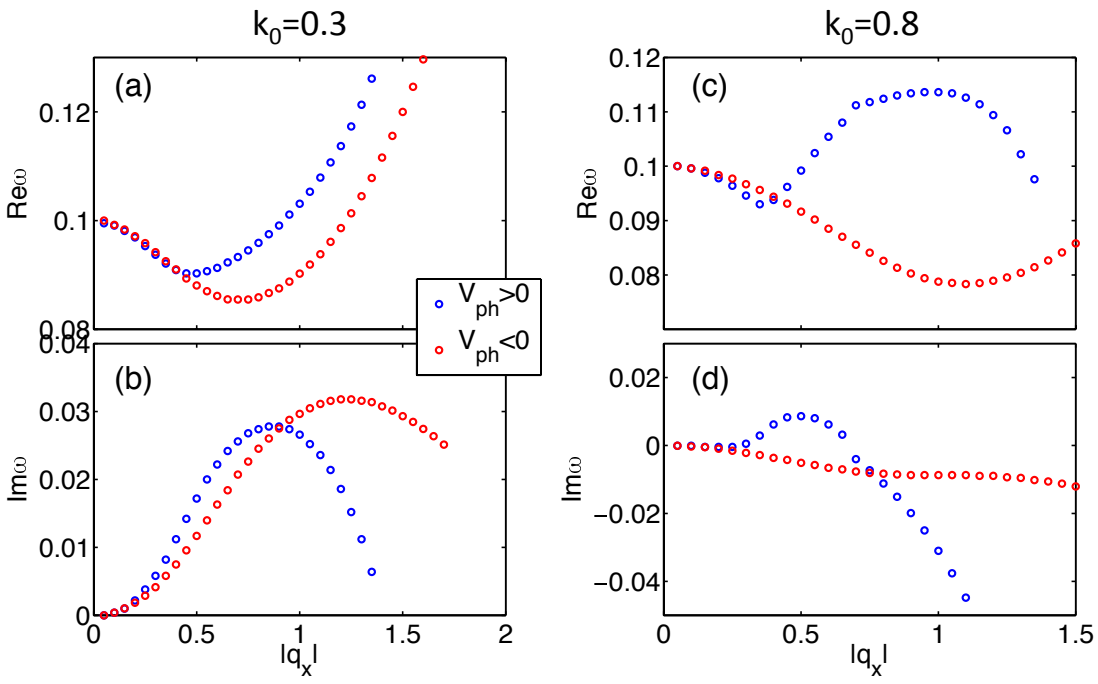

Fig. 4: Dispersion relations of GAMs coupling with drift wave turbulence. The eigenfrequencies, (a), (c), and the growth rates, (b), (d), are shown for the cases of $k_0 = 0.3$ and 0.8, respectively.

into the barrier, and the turbulence penetration occurs with the GAM frequency. When the curvature of the mean flow is larger than that of the GAM, the effect of the mean flow is strong, so that the reduction of the turbulence due to the mean flow weakens the GAMs, and the trapping effect changes. In order to have a quantitative discussion, the self-consistent treatment between the turbulence, the GAM and the mean flow is necessary, which is a future work.

5 Summary

Selection rule of the radial propagation direction of geodesic acoustic modes (GAMs) is investigated, focusing on the effect of the nonlinear coupling with the drift wave turbulence. The wave-kinetic equation for the turbulence and the fluid equation for the GAM are numerically solved, keeping the phase-space dynamics of the turbulence (turbulence trapping effect). The spatially homogeneous turbulence in a simple tokamak geometry is considered. By changing the peak turbulence radial wavenumber, we obtain the change of the propagation direction of the GAMs for the nonlinear saturated states. The wave pattern of the GAM varies to form a standing wave, outward and inward propagating waves, depending on the peak radial wavenumber of the turbulence. The impact of nonlinear coupling with turbulence is discussed by deriving the GAM dispersion relation that includes the effect of the turbulence.

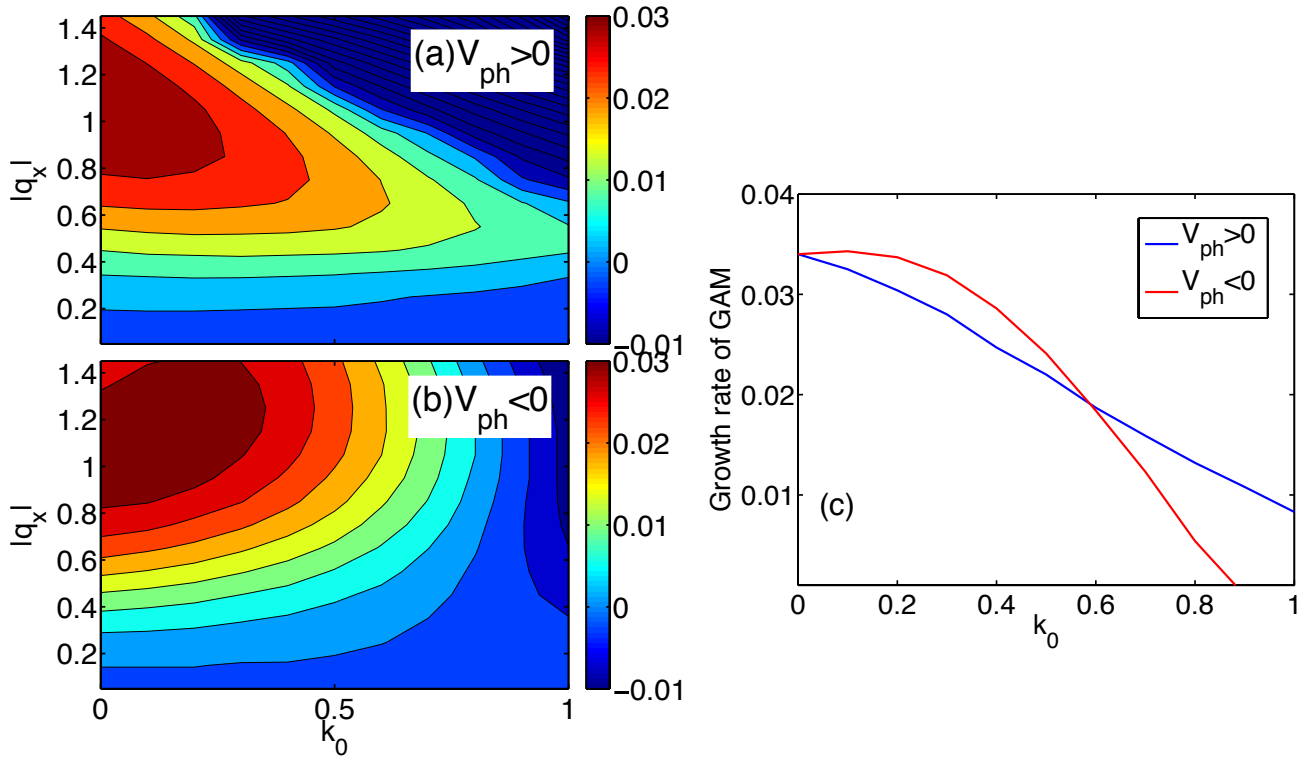

Fig. 5: Growth rates of GAMs with (a) positive and (b) negative phase velocities. (c) Maximum growth rates for q_x with positive and negative phase velocities.

Acknowledgement

This work was partly supported by a grant-in-aid for scientific research of JSPS, Japan (15H02155, 16K18335, 16H02442, 17H06089) and by the collaboration programs of NIFS (NIFS15KNST089, NIFS17KNST122) and of the RIAM of Kyushu University.

References

[1] K. Ida, S. Hidekuma, Y. Miura, T. Fujita, M. Mori, K. Hoshino, N. Suzuki, and T. Yamauchi (JFT-2M Group), Phys. Rev. Lett. **65**, 1364, (1990).

[2] P. H. Diamond, S.-I. Itoh, K. Itoh, T. S. Hahm, Plasma Phys. Control. Fusion, **47**, R35 (2005).

[3] N. Winsor, J. L. Johnson, and J. M. Dawson, Physics of Fluids **11**, 2448 (1968).

[4] K. Hallatschek and D. Biskamp, Phys. Rev. Lett. **86**, 1223 (2001).

[5] M. Sasaki, K. Itoh and S.-I. Itoh, Plasma Phys. Control. Fusion, **53** 085017 (2011).

[6] M. Sasaki, N. Kasuya, K. Itoh, Y. Kosuga, M. Lesur, K. Hallatschek and S.-I. Itoh, Nucl. Fusion, **57**, 036025 (2017).

[7] M. Sasaki, T. Kobayashi, K. Itoh, N. Kasuya, Y. Kosuga, A. Fujisawa, and S.-I. Itoh, Phys. Plasmas, **25**, 012316 (2018).

[8] M. Sasaki, K. Itoh, K. Hallatschek, N. Kasuya, M. Lesur, Y. Kosuga and S.-I. Itoh, Sci. Reports, **7**, 16767 (2017).

[9] T. Ido, Y Miura, K Kamiya, Y Hamada, K Hoshino, A Fujisawa, K Itoh, S-I Itoh, A Nishizawa, H Ogawa, Y Kusama, JFT-2M group, Plasma Phys. Control. Fusion, **48**, S41 (2006).

[10] Y. Nagashima, K. Itoh, A. Fujisawa, K. Shinohara, S.-I. Itoh, T. Ido, M. Yagi, K. Hoshino, A. Ejiri, Y. Takase, K. Uehara and Y. Miura, Plasma Rhys. Control. Fusion, **51**, 065019 (2009).

[11] Y. Xu, I. Shesterikov, M. V. Schoor, M. Vergoten, R. R. Wynants, A. Kramer-Flecken, S. Zoletnik, S. Soldatom, D. Reiser, K. Hallatschek, C. Hidalgo, and the TEXTOR Team, Plasma Phys. Control. Fusion, **53**, 095015 (2011).

[12] T. Kobayashi, M. Sasaki, T. Ido, K. Kamiya, Y. Miura, Y. Nagashima, K. Ida, S. Inagaki, A. Fujisawa, S. -I. Itoh, and K. Itoh, Phys. Rev. Lett. **120**, 045002(2018).

[13] J. C. Hildesheim, W. A. Peebles, T. A. Carter, L. Schmitz, and T. L. Rhodes, Phys. Plasmas, **19**, 022301 (2012).

[14] W.L. Zhong, Z.B. Shi, Y. Xu, X.L. Zou, X.R. Duan, W. Chen, M. Jiang, Z.C. Yang, B.Y. Zhang, P.W. Shi, Z.T. Liu, M. Xu, X.M. Song, J. Cheng, R. Ke, L. Nie, Z.Y. Cui, B.Z. Fu, X.T. Ding, J.Q. Dong, Yi Liu, L.W. Yan, Q.W. Yang, Y. Liu and HL-2A team, Nucl. Fusion, **55**, 113005 (2015).

[15] C. Silva, J.C. Hillesheim, C. Hidalgo, E. Belonohy, E. Delabie, L. Gil, C.F. Maggi, L. Meneses, E. Solano, M. Tsalas and JET Contributors, Nucl. Fusion, **56**, 106026 (2016).

[16] J. Seidl, J. Krbec, M. Hron, J. Adamek, C. Hidalgo, T. Markovic, A.V. Melnikov, J. Stockel, V. Weinzettl, M. Aftanas, P. Bilkova, O. Bogar, P. Bohm, L.G. Eliseev, P. Hacek, J. Havlicek, J. Horacek, M. Imrisek, K. Kovarik, K. Mitosinkova, R. Panek, M. Tomes and P. Vondracek, Nucl. Fusion, **57**, 126048 (2017).

[17] A D Gurchenko, E Z Gusakov, P Niskala, A B Altukhov, L A Esipov, T P Kiviniemi, T Korpilo, D V Kouprienko, S I Lashkul, S Leerink, A A Perevalov and M A Irzak, Plasma Phys. Control. Fusion, **58**, 044002 (2016).

[18] P. Simon, PhD thesis, *Investigation of geodesic acoustic mode flow oscillations using Doppler reflectometry in ASDEX Upgrade*, University de Lorraine (2017).

[19] D.F. Kong, A.D. Liu, T. Lan, Z.Y. Qiu, H.L. Zhao, H.G. Sheng, C.X. Yu, L. Chen, G.S. Xu, W. Zhang, B.N. Wan, R. Chen, W.X. Ding, X. Sun, J.L. Xie, H. Li and W.D. Liu, Nucl. Fusion, **53**, 113008 (2013).

[20] B. Liu, C. Silva, H. Figueiredo, M.A. Pedrosa, B.Ph. van Milligen, T. Pereira, U. Losada and C. Hidalgo, Nucl. Fusion, **56**, 056012 (2016).

[21] V. V. Bulanin, L. G. Askinazi, A. A. Belokurov, V. A. Kornev, V. Lebedev, A. V. Petrov, A. S. Tukachinsky, M. I. Vildjunas, F. Wagner and A. Yu Yashin, Plasma Phys. Control. Fusion, **58**, 045006 (2016).

[22] N. Miyato, Y. Kishimoto, Physics of Plasmas, **11**, 5557 (2004).

[23] X.Q. Xu, E. Belli, K. Bodi, J. Candy, C.S. Chang, R.H. Cohen, P. Colella, A.M. Dimits, M.R. Dorr, Z. Gao, J.A. Hittinger, S. Ko, S. Krasheninnikov, G.R. McKee, W.M. Nevins, T.D. Rognlien, P.B. Snyder, J. Suh and M.V. Umansky, Nuclear Fusion, **49**, 065023 (2009).

[24] Z. Gao, Phys. Plasmas, **17**, 092503 (2010).

[25] R. Hager, K. Hallatschek, Phys. Plasmas, **16**, 072503 (2009).

[26] K. Itoh, S.-I. Itoh, P. H. Diamond, A. Fujisawa, M. Yagi, T. Watari, Y. Nakashima, A. Fujisawa, Plasma Fusion Research: Rapid Communication, **1**, 037 (2006).

[27] M. Sasaki, K. Itoh, A. Ejiri, Y. Takase, Contrib. Plasma Phys. **48**, 68 (2008).

[28] F. Palermo, E. Poli, A. Bottino, A. Biancalani, G. D. Conway, and B. Scott, Phys. Plasmas, **24**, 072503 (2017).

[29] R. Hager, K. Hallatschek, Phys. Rev. Lett. **108**, 035004 (2012).

[30] M. Sasaki, K. Itoh, N. Kasuya, K. Hallatschek, S.-I. Itoh, Plasma Fusion Res. **8**, 1403010 (2013).

[31] Z. Gao, K. Itoh, H. Sanuki, and J. Q. Dong, Phys. Plasmas, **15**, 072511 (2008).

[32] M. Sasaki, K. Itoh, A. Ejiri, Y. Takase, Journal of Plasma Phys. **75**, 721 (2009).

[33] R. Singh, O. D. Gurcan, Plasma Phys. **24**, 022507 (2017).

[34] P. Kaw, R. Singh, P. H. Diamond, Plasma Phys. Control. Fusion, **44**, 51 (2002).

[35] R. Singh, P. Kaw, O. D. Gurcan, and P. H. Diamond, Plasma Phys. **21**, 102306 (2014).

[36] K. Itoh, K. Hallatschek, S.-I. Itoh, Plasma Phys. Control. Fusion, **47**, 451 (2005).

[37] A. I. Smolyakov, P. H. Diamond, and M. Malkov, Phys. Rev. Lett. **84**, 491 (2000).

[38] K. Itoh, K. Hallatschek, S.-I. Itoh, P. H. Diamond, S. Toda, **12**, 062303 (2005).

[39] M. Sasaki, K. Itoh, Y. Nagashima, A. Ejiri, Y. Takase, Phys. Plasmas, **16**, 022306 (2009).

[40] H. Sugama, T.H. Watanabe, Phys. Plasmas, **13**, 012501 (2006).

[41] M. Sasaki, K. Itoh, S.I. Itoh, N. Kasaya, Nucl. Fusion, **52**, 023009 (2012).